Journal of Hazardous Materials 190 (2011) 276–284

Contents lists available at ScienceDirect

Journal of Hazardous Materials

journal homepage: www.elsevier.com/locate/jhazmat

Synthesis of chitosan/γ-Fe_2O_3/fly-ash-cenospheres composites for the fast removal of bisphenol A and 2,4,6-trichlorophenol from aqueous solutions

Jianming Pan[a,b], Hang Yao[c], XiuXiu Li[a], Bing Wang[b], Pengwei Huo[a], Wanzhen Xu[b], Hongxiang Ou[b], Yongsheng Yan[a,*]

[a] School of Chemistry and Chemical Engineering, Jiangsu University, Zhenjiang 212013, China
[b] School of Environment, Jiangsu University, Zhenjiang 212013, China
[c] School of Materials Science and Engineering, South China University of Technology, Guangzhou 510641, China

ARTICLE INFO

Article history:
Received 5 January 2011
Received in revised form 10 March 2011
Accepted 11 March 2011
Available online 22 March 2011

Keywords:
Chitosan
Fly-ash-cenospheres
Magnetic γ-Fe_2O_3
Bisphenol A
2,4,6-Trichlorophenol adsorption

ABSTRACT

The chitosan/fly-ash-cenospheres/γ-Fe_2O_3 (CTS/γ-Fe_2O_3/FACs) magnetic composites were prepared by microemulsion process. The resulting composites were charcterized by XRD, FT-IR, SEM, TGA, DTG and VSM, and the results indicated that CTS/γ-Fe_2O_3/FACs exhibited magnetic property (M_s = 6.553 emu g^{-1}) and thermal stability, and composed of chitosan wrapping magnetic γ-Fe_2O_3 and fly-ash-cenospheres (thickness of the cross-linked chitosan was about 5.2 μm). Then the CTS/γ-Fe_2O_3/FACs were employed as adsorbents for the fast removal of bisphenol A (BPA) and 2,4,6-trichlorophenol (TCP) from aqueous solutions. The adsorption performances of CTS/γ-Fe_2O_3/FACs were investigated by batch mode experiments with respect to pH, temperature, initial concentration, contact time and binary solution system. The Langmuir isotherm model was fitted to the equilibrium data better than the Freundlich model, and the kinetic properties were well described by the pseudo-second-order equation. The effects of binary solution systems also demonstrated that BPA adsorption onto CTS/γ-Fe_2O_3/FACs was more affected by the simultaneous presence of competitive phenolic compound than that of TCP. In addition, the resulting composite reusability without obviously deterioration in performance was demonstrated by at least three repeated cycles.

1. Introduction

In recent years, endocrine disrupting chemicals (EDCs) have become one of the most relevant issues in the fields of environmental science and technology due to their potential to cause negative effects on the endocrine systems of humans and wildlife [1,2]. Bisphenols (such as bisphenol-A and bisphenol-F) and chlorophenols (such as 2,4,6-trichlorophenol, 2,4-dichlorophenol and pentachlorophenol) are typical EDCs which are widely used in industrial and agricultural activities [3]. Discharge of bisphenols or chlorophenols contaminated wastewater into aquatic environment without adequate treatment can lead to negative effect on the water quality, and pose adverse effects on the human health. Therefore, the removal of bisphenols and chlorophenols from aquatic environment is necessary and very important.

In regular monitoring, the adsorption technique that uses adsorbents is an efficient and economically feasible method for the removal of toxic EDCs such as bisphenols or chlorophenols [4]. Currently, activated carbon is the most commonly used adsorbent for the adsorption process in wastewater treatment because it has vast surface area and affinity for many organic chemicals, but it is expensive and necessitates regeneration [5,6]. Therefore, searching for alternative low-cost adsorbents that have comparable capacity to activated carbon is highly desired [7]. Recently, a variety of low-cost adsorbents have received much more attention for these purposes. For example, clay and clay composites [8–10], soils and river sediments [11,12], fly-ash and surface altered fly-ash [13,14] have been used as adsorbents for the adsorption of bisphenols and chlorophenols from aqueous solutions. Fly-ash is a by-product produced during the combustion of coal in the thermal power plants [15]. In view of converting wastes generated in some prime industries to suitable materials with practical utility, great efforts are being made to explore novel applications for fly-ash prior to disposal. Possessing of enriched SiO_2 and a portion of unburned carbon, fly-ash could be a potential adsorption material in water pollution treatment [15].

Moreover, in order to solve the difficulty in collecting adsorbents from their dispersing media, special attention has been directed to the combination of iron oxide magnetic nanoparticles and conventional adsorbents. Liu et al. prepared attapulgite/Fe_3O_4

* Corresponding author. Tel.: +86 511 8890683; fax: +86 511 88791800.
E-mail address: zhenjiangpjm@126.com (Y. Yan).

0304-3894/$ – see front matter © 2011 Elsevier B.V. All rights reserved.
doi:10.1016/j.jhazmat.2011.03.046

magnetic adsorbent by co-precipitation technique in the aqueous suspension of attapulgite pre-modified with $FeCl_3$ [16]. Liu's group attached magnetic Fe_3O_4 on carbon nanotubes by a polyol-medium solvothermal method using oleate as an interlinker molecule [17]. Cao et al. presented a work that magnetic P zeolites were hydrothermally synthesized by adding magnetic Fe_3O_4 particles during the crystallization [18]. Therefore, when combining iron oxide magnetic nanoparticles with conventional adsorbents, the resultant magnetic composites could be the promising multifunctional candidates for the adsorption and separation process.

Herein, we report an effective method to achieve magnetic composites via chitosan (CTS) enwrapping nanosized γ-Fe_2O_3 and fly-ash-cenospheres. And obtained magnetic composites (CTS/γ-Fe_2O_3/FACs) were analyzed and characterized by FT-IR, SEM, TGA, VSM and XRD. Bisphenol-A (BPA) and 2,4,6-trichlorophenol (TCP), as a typical bisphenol and chlorophenol, respectively, were selected as model pollutants to examine the performance of CTS/γ-Fe_2O_3/FACs in single and binary solutions by batch mode experiments.

2. Experimental

2.1. Materials

Fly-ash-cenospheres (FACs) were friendly supported by China Power Yaomeng Power Co. Ltd. (Henan, China). Chitosan (CTS) with 98% deacetylation and an average molecular weight of 6×10^4 g mol^{-1} was supplied by Yuhuan Biomedical Corp. (Zejiang, China). Commercially available magnetic γ-Fe_2O_3 (30 nm outer diameters; 99.5% purity), bisphenol-A (BPA) and 2,4,6-trichlorophenol (TCP) were obtained from Aladdin reagent Co., Ltd. (Shanghai, China). Twenty-five percent (v/v) of glutaraldehyde used as the cross-linking agent was provided by Shanghai Tianlian Fine Chemical Industry Co., Ltd. (Shanghai, China). Sorbitan monooleate (Span-80) and paraffin liquid were obtained from Sinopharm Chemical Reagent Co., Ltd. (Shanghai, China). Deionized ultrapure water (DUW) was purified with a Purelab ultra (Organo, Tokyo, Japan).

2.2. Instruments

Infrared spectra (4000–400 cm^{-1}) were recorded on a Nicolet NEXUS-470 FTIR apparatus (USA). The identification of crystalline phase was performed using a Rigaku D/max-γB X-ray diffractometer (XRD) with monochromatized Cu Kα radiation over the 2θ range of 20–80° at a scanning rate of 0.02° s^{-1}. The morphology of CTS/γ-Fe_2O_3/FACs was observed by a scanning electron microscopy (SEM, S-4800). Magnetic measurements were carried out using a VSM (7300, Lakeshore) under a magnetic field up to 10 kOe. TGA and DSC of samples were performed for powder samples (about 10 mg) using a Diamond TG/DTA instruments (PerkinElmer, USA) under a nitrogen atmosphere up to 800 °C with a heating rate of 5.0 °C min^{-1}.

2.3. Preparation of CTS/γ-Fe2O3/FACs

The preparation process of CTS/γ-Fe_2O_3/FACs was followed the literature [19] with more modifications. Briefly, 1.0 g of chitosan was dissolved in 50 mL of 0.1 mol L^{-1} HAc aqueous solution under a vigorous stirring for 0.5 h at room temperature. Subsequently, 0.3 g of magnetic nanosized γ-Fe_2O_3 and 0.8 g of fly-ash-cenospheres were added into the colloidal mixture and the reaction system was continued to be stirred for 1.5 h. Then 100 mL of paraffin oil containing 5% of Span-80 were slowly added into the prepared mixture under stirring. After 30 min of emulsification, 5.0 mL of 25% (v/v) glutaraldehyde was added dropwise into the mixture. Then the cross-linking reaction was continued for 90 min in a water bath at 40 °C under a nitrogen atmosphere. Next step, the pH of the mixed system was adjusted to 9.0–10 by using 1.0 mol L^{-1} $NH_3 \cdot H_2O$ and kept in a water bath for a further 1.0 h at 70 °C. Finally, the resulting brown precipitate was collected by Nd–Fe–B permanent magnet. After washed several times by n-hexane, methanol and DUW, CTS/γ-Fe_2O_3/FACs composites were dried at 60 °C under atmospheric condition.

In comparison, chitosan enwrapping nanosized γ-Fe_2O_3 composites (CTS/γ-Fe_2O_3) were also prepared as a blank in parallel but without the addition of fly-ash-cenospheres.

2.4. Single adsorption studies

The experimental parameters such as pH, temperature, initial concentration, contact time on the removal of TCP and BPA were studied in a batch mode of operations. For this purpose, the adsorption tests were performed by using polycarbonate cylindrical cells with a lid, a definite amount of adsorbent and a fixed volume of the aqueous dye solution. After the desired time, CTS/γ-Fe_2O_3/FACs composites were isolated by an external magnetic field, and the concentrations of BPA and TCP in the solvent phase were determined with UV–vis spectrophotometer. The maximum absorbance values were set at 276 nm for BPA and 292 nm for TCP, respectively. Moreover, the equilibrium adsorption capacity (Q_e, mg g^{-1}) was calculated.

2.5. Binary adsorption studies

The first step was to examine the adsorption of BPA at equilibrium (concentration of BPA ranging from 80 to 300 mg L^{-1}) in the presence of TCP (50 mg L^{-1} or 80 mg L^{-1}). For the next step, a series of binary solutions where the concentration of BPA was fixed at 50 mg L^{-1} or 80 mg L^{-1}, and concentration of TCP was varied from 100 to 300 mg L^{-1}. These binary solutions were also agitated at 300 rpm for 3.0 h. Equilibrium concentrations of BPA and TCP in the various binary solutions were determined by UV–vis spectrophotometer through the multi-component determination option. In this experiment, the adsorption temperature was at 298 K, and the solution pH was 7.0 for the first step and 5.0 for the second step, respectively.

2.6. Desorption and reuse studies

Desorption study was conducted using methanol/acetic acid (95:5, v/v) solution as desorption eluent. Adsorption was first conducted using the optimal procedure in Section 2.4. Then the CTS/γ-Fe_2O_3/FACs with adsorbed TCP or BPA were separated rapidly from the solutions by Nd–Fe–B permanent magnet. Subsequently, the supernatant solutions were discarded and the CTS/γ-Fe_2O_3/FACs composites were washed with 2× 2.0 mL of acetonitrile. Finally, the TCP or BPA were desorbed from the CTS/γ-Fe_2O_3/FACs with 2× 2.5 mL of methanol solution containing 5.0% acetic under the action of ultrasound. To investigate the regeneration of the adsorbent, the CTS/γ-Fe_2O_3/FACs after desorption was reused in adsorption experiments and the process was repeated for three times.

3. Results and discussion

3.1. Characterization of CTS/γ-Fe2O3/FACs

The FT-IR spectra of the CTS (a), γ-Fe_2O_3 (b), FACs (c) and CTS/γ-Fe_2O_3/FACs (d) were measured and shown in Fig. 1, respectively. The main functional groups of the predicted structure can be observed with corresponding infrared absorption peaks. From

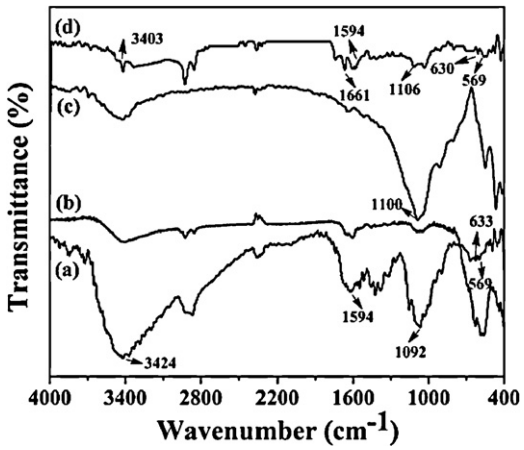

Fig. 1. FT-IR spectrum of the CTS (a), γ-Fe_2O_3 (b), FACs (c) and CTS/γ-Fe_2O_3/FACs (d).

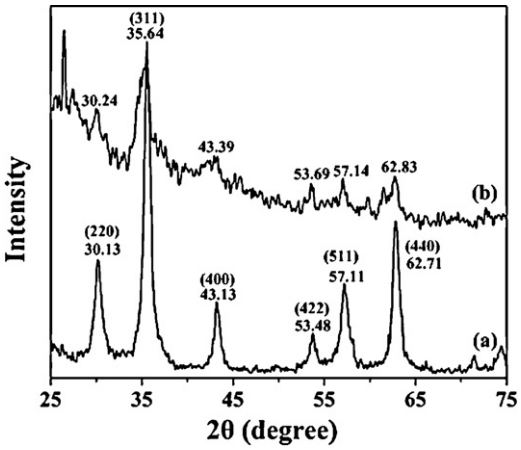

Fig. 2. X-ray diffraction (XRD) patterns of γ-Fe_2O_3 (a) and CTS/γ-Fe_2O_3/FACs (b).

the CTS spectrum, the absorption peaks at 1594 and 1092 cm^{-1} were attributed to the bending vibrations of N–H and skeletal vibration of C–O. And the strong and wide peak around 3424 cm^{-1} was assigned to the stretching vibrations of N–H and O–H in CTS. But this characteristic absorption peak shifted to 3403 cm^{-1} and obviously became narrow for CTS/γ-Fe_2O_3/FACs. Moreover, the characteristic feature of δ_sN–H at 1594 cm^{-1} decreased in the spectrum of CTS/γ-Fe_2O_3/FACs and a new sharp peak at 1661 cm^{-1} appeared, indicating that the cross-linking reaction took place on the $-NH_2$ from CTS to form Schiff base [19]. The peaks around 630 cm^{-1} and 569 cm^{-1}, which were existed in the FT-IR spectrum of γ-Fe_2O_3 and CTS/γ-Fe_2O_3/FACs, indicated the presence of Fe–O group. This result confirmed that the introduction of γ-Fe_2O_3 into the cross-linked CTS has been occurred [20]. The absorption peak at 1110 cm^{-1} of FACs corresponded to the Si–O–Si bond, which was also obtained by CTS/γ-Fe_2O_3/FACs.

Fig. 2 shows the X-ray diffraction (XRD) patterns of γ-Fe_2O_3 (a) and CTS/γ-Fe_2O_3/FACs (b). In the 2θ range of 25–75°, six characteristic peaks corresponded to maghemite (2θ = 30.13°, 35.64°, 43.13°, 53.48°, 57.11° and 62.71°) were observed in the γ-Fe_2O_3, and the peak positions could be indexed to (2 2 0), (3 1 1), (4 0 0), (4 2 2), (5 1 1) and (4 4 0) (JCPDS card (39-1346) for Fe_2O_3) [20]. Moreover, the corresponding peaks were well present in the pattern of CTS/γ-Fe_2O_3/FACs, but were shifted to lower wavenumbers than those of γ-Fe_2O_3. The results suggested that γ-Fe_2O_3 was introduced into cross-linked CTS/FACs with no change for its crystal structure.

The morphology of FACs (a), CTS/γ-Fe_2O_3/FACs (b) and cross section of CTS/γ-Fe_2O_3/FACs (c) were observed by SEM. As can be observed in Fig. 3a, the FACs is rough-faced and spherical morphology. The sphere has a diameter near 123 μm. In Fig. 2b, the SEM micrograph of CTS/γ-Fe_2O_3/FACs presented relatively smooth surface and the diameter was near 140 μm, indicating that the CTS/γ-Fe_2O_3/FACs composites were coated with cross-linked CTS. Moreover, many pores were existed on the surface, which may be benefit for BPA and TCP to be trapped and adsorbed within a short time. According to the cross section of composite adsorbent (Fig. 3b), the average thickness of the wall for FACs was 2.7 μm, and the thickness of the cross-linked CTS for CTS/γ-Fe_2O_3/FACs was about 5.5 μm. This result was in agreement with the size of FACs and CTS/γ-Fe_2O_3/FACs.

Fig. 4a shows the magnetic hysteresis loop of CTS/γ-Fe_2O_3/FACs, and the general shape and trend of the curve indicated that CTS/γ-Fe_2O_3/FACs was super paramagnetic [21]. It was obvious that the saturation magnetization (M_s) values obtained at room temperature were 6.553 emu g^{-1} for CTS/γ-Fe_2O_3/FACs, implying a relative strong magnetic response to the external magnetic field. Moreover, the results from Fig. 4b strongly suggested that the remained magnetic force in CTS/γ-Fe_2O_3/FACs could be attracted by an external magnetic field effectively. The results also illustrated that CTS/γ-Fe_2O_3/FACs was a feasible magnetic separation carrier.

Fig. 5 shows the TGA and DTG curves of the FACs, γ-Fe_2O_3 and CTS/γ-Fe_2O_3/FACs. As shown in Fig. 5, the FACs cannot be easily decomposed even at high temperature (800 °C), indicating the thermal stability. For γ-Fe_2O_3, it showed little weight loss (3.36%) which can be ascribed to the evaporation of water molecules. Moreover, a wide exothermic peak ranged from 465 °C to 650 °C was shown in DTG curve of γ-Fe_2O_3 while no corresponding changes in TGA

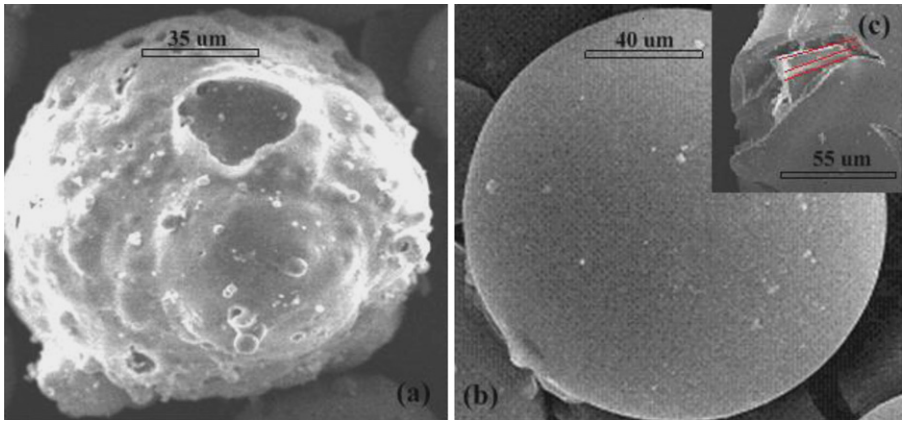

Fig. 3. Micrographs from a scanning electron microscopy of FACs (a), CTS/γ-Fe_2O_3/FACs (b) and cross section of CTS/γ-Fe_2O_3/FACs (c).

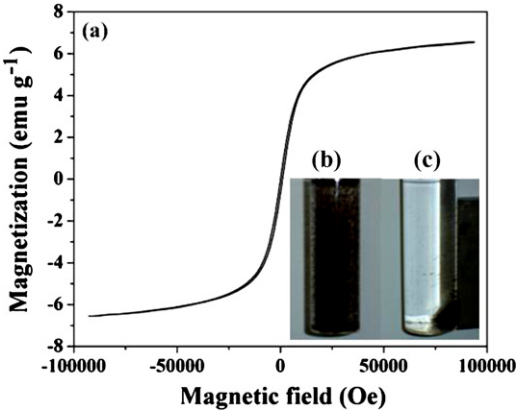

Fig. 4. Magnetization curve of CTS/γ-Fe_2O_3/FACs (a), photographs of CTS/γ-Fe_2O_3/FACs suspended in water in the absence (b) and in the presence (c) of an externally placed magnet.

curve. Some authors attributed this observation to the phase transition from γ-Fe_2O_3 to α-Fe_2O_3 [22,23]. For CTS/γ-Fe_2O_3/FACs, total weight loss was 45.08% from 25 °C to 800 °C. Compared with γ-Fe_2O_3, the characteristic peak of the phase transition from γ-Fe_2O_3 to α-Fe_2O_3 disappeared in the DTG curve of CTS/γ-Fe_2O_3/FACs due to their rigid structure [19]. Thus, the remaining mass for CTS/γ-Fe_2O_3/FACs was attributed to the thermal resistance of FACs and γ-Fe_2O_3 particles.

3.2. Effect of pH on adsorption of BPA and TCP

In previous studies, the fact that neutral molecules of phenolic compound are benefit for the adsorption process has also been reported [24–26]. Then, the effect of pH on the adsorption of BPA and TCP and the effect of initial pH on final pH were shown in Fig. 6, respectively. From Fig. 6, adsorption of neutral BPA at pH 7.0 (at pH 5.0 for TCP) onto CTS/γ-Fe_2O_3/FACs did not cause any change in pH. And it was expected that adsorption capacity of BPA attained maximum value of 8.549 mg g^{-1} at pH 7.0 (25.91 mg g^{-1} at pH 5.0 for TCP). Thus, pH 7.0 for BPA and 5.0 for TCP were selected for the following studies. At a higher pH, the repulsion of the negatively charged BPA or TCP species and the dissociation of functional groups of adsorbents may decrease the interaction of adsorption system. Accordingly, at a lower pH, the functional groups of CTS/γ-Fe_2O_3/FACs and molecules of phenolic compound positively charged, electrostatic repulsion was also not benefit for the adsorption system. The results strongly suggested that BPA and TCP were trapped by CTS/γ-Fe_2O_3/FACs through

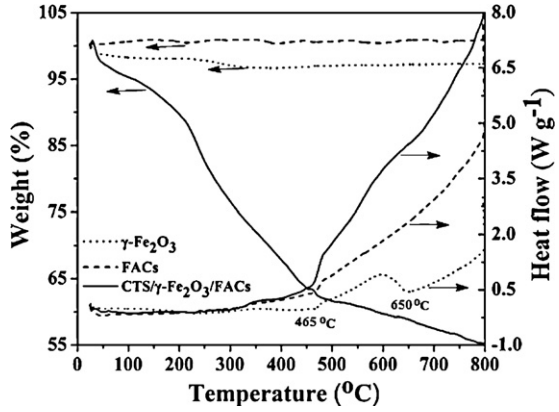

Fig. 5. TGA and DTG curves of the FACs, γ-Fe_2O_3 and CTS/γ-Fe_2O_3/FACs.

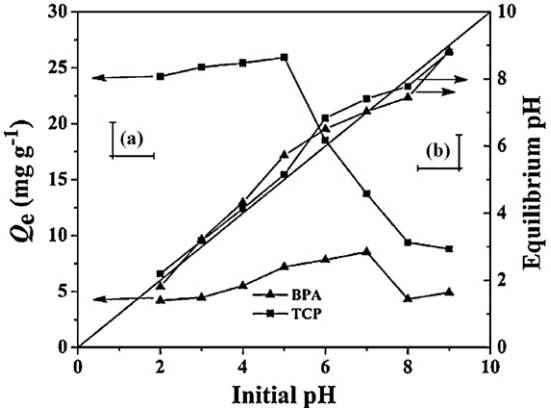

Fig. 6. (a) Effect of pH on adsorptive removal of BPA and TCP and (b) effect of initial pH on equilibrium pH.

the hydrophobic interaction and the hydrogen-bonding interaction simultaneously.

3.3. Effects of contact time at different initial concentrations and temperatures

A study of the effect of contact time on the adsorption of BPA (a) and TCP (b) onto CTS/γ-Fe_2O_3/FACs at different initial concentrations and temperatures are shown in Fig. 7. Moreover, in order to show the validity of the composite adsorbent, three types of adsorbents (γ-Fe_2O_3, FACs and CTS/γ-Fe_2O_3) were also selected for the adsorption of BPA (Fig. 7a) and TCP (Fig. 7b). It was observed that with the increase of temperature and initial concentration, the adsorption rate and adsorption capacity increased obviously. It was possible that the initial concentration of phenolic compound molecules (BPA or TCP) provided the necessary driving force to overcome the resistances of mass transfer between the aqueous phases and the solid phase [26]. Furthermore, higher temperature may provide more chances for phenolic compound molecules to pass the external boundary layer, and produced the enlargement of pore volume and surface area enabling phenolic compound molecules to penetrate further [27]. Compared with CTS/γ-Fe_2O_3/FACs, γ-Fe_2O_3, FACs and CTS/γ-Fe_2O_3 possessed lower adsorption capacity and slower adsorption rate. However, when the FACs were introduced into CTS/γ-Fe_2O_3, the equilibrium adsorption capacity (Q_e) for both BPA and TCP was increased obviously. The similar result has been observed by Zhu's group [19], and it was believed that more available sites, larger surface area and smaller pore diameter have been provided by the introduction of microparticles (such as FACs) into the cross-linked chitosan [20]. In addition, the adsorption capacity for BPA and TCP both followed the order: CTS/γ-Fe_2O_3/FACs > CTS/γ-Fe_2O_3 > FACs > γ-Fe_2O_3, suggesting the cross-linked CTS and FACs played vital role in the increase of adsorption capacity. The essential function of γ-Fe_2O_3 could be only the magnetic source.

3.4. Adsorption kinetics

The pseudo-first-order equation [28], pseudo-second-order equation [29] and intraparticle diffusion model [30], which can be expressed by Eqs. (1)–(3), respectively, were used to describe the rate of solute uptake at the solid–solution interface.

$$Q_t = Q_e - Q_e e^{-\kappa_1 t} \quad (1)$$

$$Q_t = \frac{k_2 Q_e{}^2 t}{1 + k_2 Q_e t} \quad (2)$$

$$Q_t = k_i t^{0.5} + C \quad (3)$$

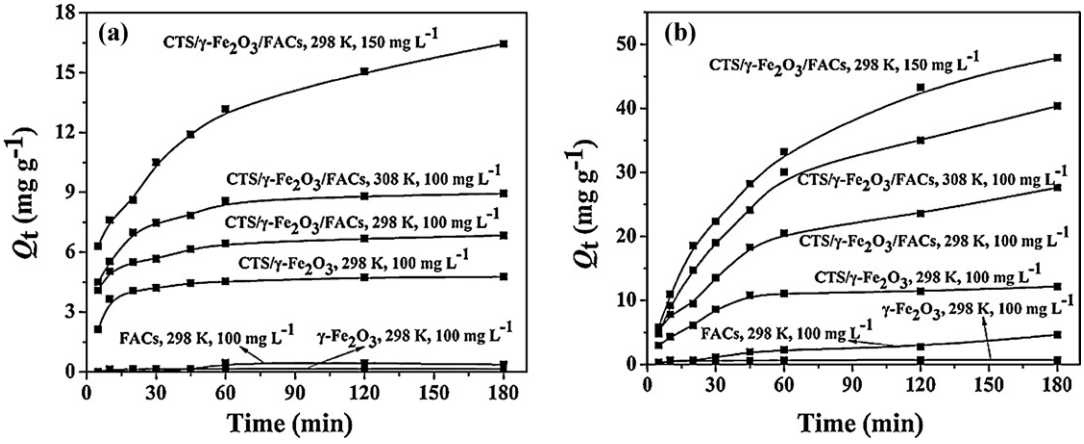

Fig. 7. Effects of contact time at different initial concentrations and temperatures on adsorptive removal of BPA (a) and TCP (b).

where Q_e and Q_t are the amount of adsorbate (mg g^{-1}) onto adsorbent at the equilibrium and time t (min), respectively. Values of k_1 (L min^{-1}) and k_2 (g mg^{-1} min^{-1}) are calculated from the plot of $\ln(Q_e - Q_t)$ versus t and t/q_t versus t, respectively. k_i is the intraparticle diffusion rate constant (mg g^{-1} min$^{-0.5}$), C (mg g^{-1}) is the intercept of intraparticle diffusion model.

The adsorption rate constants and regression values from two rate equations are summarized in Table 1. The non-linear regression plots of pseudo-first-order kinetic model, pseudo-second-order kinetic model and intraparticle diffusion model are shown in Fig. 8. The applicability of the kinetic models to the adsorption behaviours was studied by judging the correlation coefficient (R^2) as well as the experimental and calculated data of equilibrium adsorption capacity (Q_e).

The adsorption of BPA followed pseudo-second-order kinetics because of the favourable fit between experimental and calculated values of Q_e (R^2 values above 0.9850 at different conditions). From Fig. 8a, pseudo-second order kinetic lines of BPA deviated substantially from the experimental points around the first 20 min. The observed deviation from experimental data could be attributed to the sharp fall in concentration gradient after the initial rapid adsorption of BPA molecules onto the large amount of vacant binding sites and not concentration dependent [20,31]. Within this time period, it was believed that there was a switch between mass transfer diffusion control and pore diffusion control, and a change in adsorption mechanism may have occurred after the first 20 min for BPA adsorption [32,33]. For TCP adsorption onto CTS/γ-Fe_2O_3/FACs, the calculated equilibrium adsorption capacity ($Q_{e,c}$) agreed better with the experimental value ($Q_{e,exp}$) for pseudo-first-order kinetic model (Table 1). However, the values of R^2 of pseudo-first-order kinetic model were lower than those of pseudo-second-order kinetic model, indicating that the pseudo-second-order kinetic model was more valid to clarify the behaviours of TCP adsorption. From Fig. 8b, non-linear forms of pseudo-second-order kinetic model studied at different conditions also showed the better fit than pseudo-first-order kinetic model, indicating the adsorption of TCP was due to chemisorption. From Fig. 8a, the results also suggested that pseudo-first-order kinetic model would be applicable only over the initial stage of the adsorption process. The regression analysis of intraparticle diffusion model showed that the correlation coefficient values (R^2) for BPA and TCP were lower than 0.96, indicating that more than one process affected the BPA and TCP adsorption onto CTS/γ-Fe_2O_3/FACs.

In order to gain more information about the mechanism and rate-controlling steps affecting the kinetics of adsorption, pore diffusion and film diffusion were also used to investigate the adsorption process. And the pore diffusion and film diffusion equations [34] can be expressed by Eqs. (4) and (5), respectively.

$$\frac{Q_t}{Q_e} = 6\left(\frac{D_1}{\pi a^2}\right)^{0.5} t^{0.5} + C \tag{4}$$

$$Bt = -0.4997 - \ln\left(1 - \frac{Q_t}{Q_e}\right) \tag{5a}$$

$$B = \pi^2 \frac{D_2}{a^2} \tag{5b}$$

a (μm) is the average radius of the CTS/γ-Fe_2O_3/FACs particle. D_1 and D_2 are the film diffusion coefficient (μm^2 S^{-1}) and pore diffusion coefficient (μm$^{2\,-1}$), respectively.

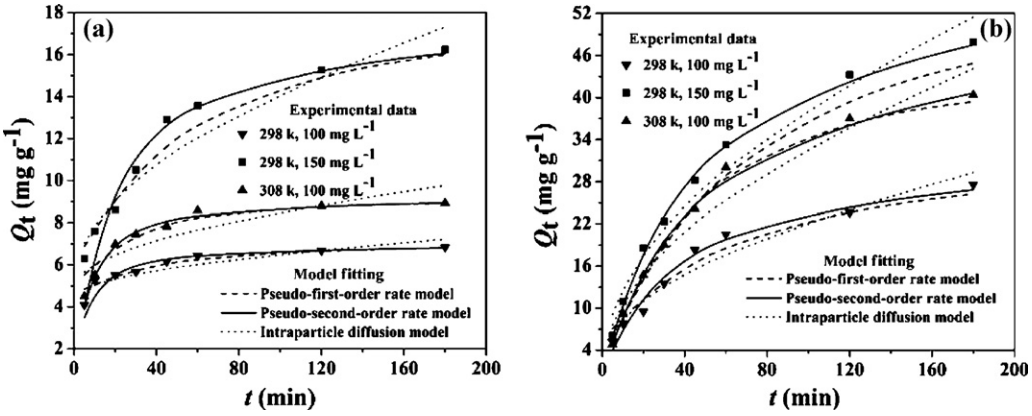

Fig. 8. Kinetic models of the effects of initial concentrations and temperatures for adsorption of BPA (a) and TCP (b) onto CTS/γ-Fe_2O_3/FACs.

Table 1
Kinetic constants for the pseudo-first-order model, pseudo-second-order model and intra-particle diffusion model.

Adsorbates	T (K)	C_0 (mg L^{-1})	$Q_{e,exp}$ (mg g^{-1})	Pseudo-first-order kinetic model			Pseudo-second-order kinetic model			Intra-particle diffusion model		
				$Q_{e,c}$ (mg g^{-1})	k_1 (L min^{-1})	R^2	$Q_{e,c}$ (mg g^{-1})	k_2 ($\times 10^{-2}$ g mg^{-1} min^{-1})	R^2	k_i (mg g^{-1} min$^{-0.5}$)	C (mg g^{-1})	R^2
BPA	298	100	6.839	2.245	0.0236	0.9562	6.998	2.818	0.9995	0.2110	4.398	0.8066
	298	150	16.45	10.44	0.0174	0.9899	17.61	0.3288	0.9937	0.9206	4.966	0.9608
	308	100	8.930	3.981	0.0305	0.9451	9.259	1.677	0.9997	0.3676	4.836	0.7770
TCP	298	100	27.60	22.21	0.0155	0.9512	32.26	0.0854	0.9852	2.035	1.974	0.9491
	298	150	50.90	46.40	0.0166	0.9729	60.98	0.0372	0.9919	3.656	2.720	0.9622
	308	100	40.37	47.54	0.0285	0.9806	52.91	0.0370	0.9927	3.367	2.370	0.9424

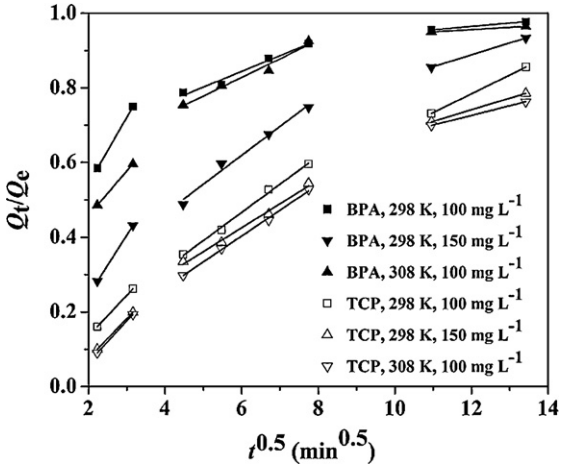

Fig. 9. Plots of Q_t/Q_e versus $t^{0.5}$ for adsorption of BPA and TCP onto CTS/γ-Fe_2O_3/FACs.

The plots of Q_t/Q_e versus $t^{0.5}$ for adsorption of BPA and TCP onto CTS/γ-Fe_2O_3/FACs were shown in Fig. 9. It was observed that there were three sections in the curves represented by straight lines. The slopes of three sections followed the order the initial section > the second section > the last section, indicating the BPA and TCP were transported to macro-, meso- and then slowly diffused into micropores [33,35]. According to the values of intercept for pore diffusion, the plots of Bt versus t for BPA and TCP (figure not shown) did not pass through the origin (but intersected the y-axis between −0.0497 and 0.7250 for BPA, −0.3119 and −0.2606 for TCP) indicating that external mass transfer was the rate-limiting process at the beginning of the adsorption process [33].

All the values of k_i, D_1 and D_2 at different initial concentrations and temperatures are shown in Table 2. The data in Table 2 showed that the film and intraparticle diffusion increased with increasing initial phenolic compound concentration and solution temperature while the pore diffusion decreased. Moreover, the results also showed that the pore diffusion was faster than the film diffusion, indicating the diffusion process was controlled by film diffusion.

3.5. Adsorption isotherm

Adsorption isotherms are basically important to describe the non-linear and dynamic equilibrium between the adsorbed solute on the adsorbent and solute in the solution at a constant temperature, and the analysis of isotherm data is critical in optimizing the use of adsorbents [36]. Then the equilibrium data in single solution system were fitted to the Langmuir [26] and Freundlich [37] isotherm models. The applicability of the isotherm models to the adsorption behaviours was studied by judging the correlation coefficient (R^2) and a normalized standard deviation $\Delta Q(\%)$. $\Delta Q(\%)$ is calculated using

$$\Delta Q(\%) = 100\sqrt{\frac{\sum[(Q_{exp} - Q_{cal})/Q_{exp}]^2}{N-1}} \quad (6)$$

where Q_{exp} and Q_{cal} are experimental and calculated amount of adsorbate adsorbed onto adsorbent, respectively, and N is the number of measurements made.

The nonlinear form of the Langmuir and Freundlich isotherm models was expressed by the following equations, respectively:

$$Q_e = \frac{K_L Q_m C_e}{1 + K_L C_e} \quad (7)$$

$$Q_e = K_F C_e^{1/n} \quad (8)$$

Table 2
Intraparticle rate parameters and diffusion coefficients at different initial concentrations and temperatures.

Adsorbates	T (K)	C_0 (mg L^{-1})	Film diffusion			Pore diffusion		
			D_1 (μm^2 S^{-1})	Intercept	R^2	D_2 (μm^2 S^{-1})	Intercept	R^2
BPA	298	100	2.96×10^{-3}	0.6284	0.8066	5.77×10^{-2}	0.7250	0.9401
	298	150	1.00×10^{-2}	0.2500	0.9366	4.83×10^{-2}	−0.0497	0.9818
	308	100	5.12×10^{-3}	0.5224	0.7779	5.50×10^{-2}	0.5681	0.8558
TCP	298	100	1.09×10^{-2}	0.0612	0.9491	3.62×10^{-2}	−0.2606	0.9624
	298	150	1.26×10^{-2}	0.0106	0.9720	3.05×10^{-2}	−0.3119	0.9887
	308	100	1.24×10^{-2}	0.0049	0.9424	2.90×10^{-2}	−0.3066	0.9442

Table 3
Adsorption isotherm constants for BPA and TCP.

Adsorption isotherm models	Constants	BPA			TCP		
		298 K	308 K	318 K	298 K	308 K	318 K
Langmuir equation	R^2	0.9959	0.9954	0.9963	0.9854	0.9881	0.9834
	$Q_{m,c}$ (mg g^{-1})	77.99	90.09	103.1	106.4	153.8	172.4
	K_L (L mg^{-1})	0.0021	0.0023	0.0022	0.0066	0.0067	0.0087
	ΔQ (%)	4.03	3.78	4.26	3.12	2.47	3.55
Freundlich equation	R^2	0.9953	0.9951	0.9949	0.9771	0.9803	0.9760
	K_F (mg g^{-1})	0.2384	0.3130	0.3455	1.331	1.826	2.607
	$1/n$	0.8506	0.8459	0.8519	0.7305	0.7462	0.7284
	ΔQ (%)	4.77	3.19	5.42	2.85	4.35	4.38

where C_e is the equilibrium concentration of adsorbate (mg L^{-1}), Q_m is the maximum adsorption capacity of the adsorbent, K_L is the affinity constant. Where K_F (mg g^{-1}) and n are both the adsorption equilibrium constants.

The adsorption isotherm constants at three temperatures are listed in Table 3. From Table 3, it was also observed that the values of $1/n$ were all less than 1.0 for all temperatures, indicating that the BPA and TCP adsorption onto the CTS/γ-Fe_2O_3/FACs was favourable [38]. Moreover, comparison of Langmuir and Freundlich isotherm models for BPA and TCP adsorption onto CTS/γ-Fe_2O_3/FACs using non-linear regression were also illustrated in Figure SI (Supporting Information). By fitting the experimental data with Langmuir and Freundlich isotherm equations, it was also found that Langmuir isotherm model fitted the equilibrium data significantly better than the Freundlich model, indicating monolayer molecular adsorption for BPA and TCP.

3.6. Competitive adsorption in binary solution systems

To study the adsorption interaction between BPA and TCP, the effect of competitive adsorption of BPA and TCP onto CTS/γ-Fe_2O_3/FACs at different initial concentrations is also listed in Table 4. The values of Q_e^b(binary solution system)/Q_e^s(single solution system) for both BPA (0.5159 and 0.4316 when the addition of 50 and 80 mg L^{-1} of TCP, respectively) and TCP (0.7243 and 0.6304 when the addition of 50 and 80 mg L^{-1} of BPA, respectively) were found to be less than 1.0, suggesting that simultaneous presence of both phenolic compound molecules reduced the adsorption through competition for binding sites on the CTS/γ-Fe_2O_3/FACs [39]. Moreover, the values of Q_e^b/Q_e^s for TCP were higher than those of BPA, indicating that BPA adsorption onto CTS/γ-Fe_2O_3/FACs was more affected by the simultaneous presence of competitive phenolic compound molecules than that of TCP [40]. The total adsorption capacity in binary solution systems was shown in Figure SI. The total adsorption capacity reduced with the increase of competitive TCP while slightly increased in the presence of competitive BPA. The results confirmed that the preferential adsorption by CTS/γ-Fe_2O_3/FACs was given to the TCP.

Moreover, at the higher concentration of competitive phenolic compound, the values of Q_e^b/Q_e^s also lead to a slight decrease, implying that the behaviours of competitive adsorption were enhanced at higher concentration of competitive phenolic compound.

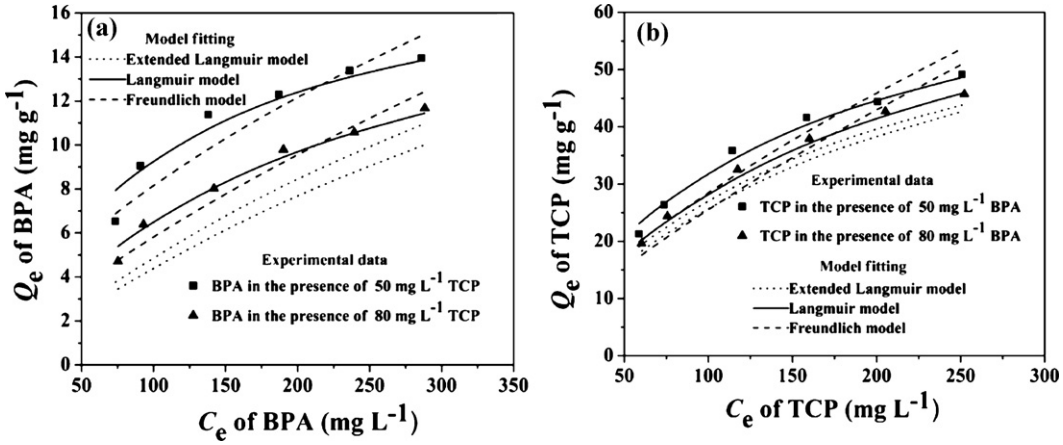

Fig. 10. Isotherm plots of experimental data and three isotherm models for (a) BPA in the presence of TCP and (b) TCP in the presence of BPA onto CTS/γ-Fe_2O_3/FACs.

Table 4
Effect of competitive adsorption of BPA and TCP onto CTS/γ-Fe_2O_3/FACs at different initial concentrations.

C_0 (BPA) (mg L^{-1})	C_0 (TCP) = 50 mg L^{-1}		C_0 (TCP) = 80 mg L^{-1}		C_0 (TCP) (mg L^{-1})	C_0 (BPA) = 50 mg L^{-1}		C_0 (BPA) = 80 mg L^{-1}	
	Q_e (BPA) (mg g^{-1})	Q_e (TCP) (mg g^{-1})	Q_e (BPA) (mg g^{-1})	Q_e (TCP) (mg g^{-1})		Q_e (TCP) (mg g^{-1})	Q_e (BPA) (mg g^{-1})	Q_e (TCP) (mg g^{-1})	Q_e (BPA) (mg g^{-1})
80	6.528	12.81	4.712	19.62	80	21.31	2.891	18.30	4.712
100	9.057	11.66	6.990	18.43	100	26.37	2.255	21.55	3.688
150	11.98	10.44	8.018	16.54	150	35.86	1.716	28.69	2.311
200	12.99	9.661	9.799	14.87	200	41.61	1.271	34.53	1.648
250	13.88	8.594	10.57	12.64	250	49.39	1.095	38.82	1.106
300	13.96	8.175	11.68	11.59	300	49.17	0.776	42.80	0.078

Then the isotherm data of the binary solution systems were analyzed using the Langmuir, Freundlich and extended Langmuir models, and the plots of experimental data and three isotherm models for (a) BPA in the presence of TCP and (b) TCP in the presence of BPA onto CTS/γ-Fe_2O_3/FACs are shown in Fig. 10.

The extended Langmuir model can be expressed as [41]:

$$Q_{e,1} = \frac{Q_{m,1}K_{L,1}C_{e,1}}{1 + K_{L,1}C_{e,1} + K_{L,2}C_{e,2}} \quad (9a)$$

$$Q_{e,2} = \frac{Q_{m,2}K_{L,2}C_{e,2}}{1 + K_{L,1}C_{e,1} + K_{L,2}C_{e,2}} \quad (9b)$$

where $K_{L,1}$, $K_{L,2}$, $Q_{m,1}$ and $Q_{m,2}$ are the Langmuir isotherm model parameters obtained suitably from Eq. (7) in the single solute system.

According to the trend in Fig. 10, the adsorption of BPA and TCP from binary molecule solutions was best described by the Langmuir isotherm model, indicating the adsorbate molecules were adsorbed at well-defined sites and there were no interactions between molecules adsorbed on adjacent sites [40]. Moreover, the fitting curves for different concentrations of competitive phenolic compounds were nearly parallel. The similar phenomena has been observed by Sismanoglu's group, the fact that the energy of adsorption between the specific adsorbing species and the surface sites is constant and equal for each site has also been reported [42].

3.7. Desorption and reuse

To test the regeneration of the CTS/γ-Fe_2O_3/FACs, adsorption/desorption cycles were conducted with TCP and BPA. The adsorption capacities of the CTS/γ-Fe_2O_3/FACs for the TCP and BPA in the adsorption/desorption cycles are shown in Figure SI. It was observed that at the first adsorption step, the adsorption capacities for the BPA and TCP reached the values of 6.83 and 26.59 mg g^{-1}, respectively. After the desorption step, the adsorbed BPA and TCP were removed about 84.9% and 89.8%, respectively, by methanol/acetic acid (95:5, v/v) solution. The most likely explanation was that strong competitive adsorption of methanol molecules onto CTS/γ-Fe_2O_3/FACs surface. In additional, the second and the third adsorption step showed the similar dynamical shape of the first adsorption step, suggesting good retention of the activity of the CTS/γ-Fe_2O_3/FACs. It can also be seen that the total adsorption capacities of both TCP and BPA slightly decreased with increasing the using times. This could be ascribed to the fact that the regeneration process might result in the decrease of binding sites [43].

4. Conclusions

In the present investigation, CTS/γ-Fe_2O_3/FACs magnetic composites were successfully prepared and evaluated as an adsorbent for the adsorption of BPA and TCP in single and binary solution systems. The prepared CTS/γ-Fe_2O_3/FACs exhibited excellently spherical morphology, thermal stability and saturation magnetization. After capture and adsorption of BPA and TCP from aqueous solutions, CTS/γ-Fe_2O_3/FACs could be easily separated from the suspension by an external magnetic field. The Langmuir isotherm model was fitted to the equilibrium data better than the Feundlich model, and the monolayer adsorption capacities for BPA and TCP were 31.92 mg g^{-1} and 69.89 mg g^{-1} at 298 K, respectively. The kinetic properties of CTS/γ-Fe_2O_3/FACs were well described by the pseudo-second-order equation. Intraparticle diffusion (k_i) and film diffusion (D_1) increased with the increasing initial concentration and solution temperature while the pore diffusion (D_2) decreased. In binary systems, BPA adsorption onto CTS/γ-Fe_2O_3/FACs was more affected by the simultaneous presence of competitive phenolic compound molecules than that of

TCP. Furthermore, CTS/γ-Fe_2O_3/FACs magnetic composites could be regenerated and reused to adsorption of BPA and TCP again.

Acknowledgments

This work was financially supported by the National Natural Science Foundation of China (No. 21077046, No. 30970309), Ph.D. Programs Foundation of Ministry of Education of China (No. 20093227110015) and Ph.D. Innovation Programs Foundation of Jiangsu Province (No. CX10B_276Z).

Appendix A. Supplementary data

Supplementary data associated with this article can be found, in the online version, at doi:10.1016/j.jhazmat.2011.03.046.

References

[1] Z.H. Liu, Y. Kanjo, S. Mizutani, Removal mechanisms for endocrine disrupting compounds (EDCs) in wastewater treatment-physical means, biodegradation, and chemical advanced oxidation: a review, Sci. Total Environ. 407 (2009) 731–748.
[2] C. Bicchi, T. Schilirò, C. Pignata, E. Fea, C. Cordero, F. Canale, G. Gilli, Analysis of environmental endocrine disrupting chemicals using the E-screen method and stir bar sorptive extraction in wastewater treatment plant effluents, Sci. Total Environ. 407 (2009) 1842–1851.
[3] C. Basheer, H.K. Lee, Analysis of endocrine disrupting alkylphenols, chlorophenols and bisphenol-A using hollow fiber-protected liquid-phase microextraction coupled with injection port-derivatization gas chromatography–mass spectrometry, J. Chromatogr. A 1057 (2004) 163–169.
[4] K. Sun, B. Gao, Z.Y. Zhang, G.X. Zhang, X.T. Liu, Y. Zhao, B.S. Xing, Sorption of endocrine disrupting chemicals by condensed organic matter in soils and sediments, Chemosphere 80 (2010) 709–715.
[5] D. Karadag, M. Turan, E. Akgul, S. Tok, A. Faki, Adsorption equilibrium and kinetics of Reactive Black 5 and Reactive Red 239 in aqueous solution onto surfactant-modified zeolite, J. Chem. Eng. Data 52 (2007) 1615–1620.
[6] M.K. Purkait, S. DasGupta, S. De, Adsorption of eosin dye on activated carbon and its surfactant based desorption, J. Environ. Manage. 76 (2005) 135–142.
[7] H.L. Wang, W.F. Jiang, Adsorption of dinitro butyl phenol (DNBP) from aqueous solutions by fly ash, Ind. Eng. Chem. Res. 46 (2007) 5405–5411.
[8] W.T. Tsai, H.C. Hsu, T.Y. Su, K.Y. Lin, C.M. Lin, Adsorption characteristics of bisphenol-A in aqueous solutions onto hydrophobic zeolite, J. Colloid Interface Sci. 299 (2006) 513–519.
[9] B.H. Hameed, Equilibrium and kinetics studies of 2,4, 6-trichlorophenol adsorption onto activated clay, Colloids Surf. A 307 (2007) 45–52.
[10] S.H. Lin, M.J. Cheng, Adsorption of phenol and m-chlorophenol on organobentonites and repeated thermal regeneration, Waste Manage. 22 (2002) 595–603.
[11] G.M. Zeng, C. Zhang, G.H. Huang, J. Yu, Q. Wang, J.B. Li, B.D. Xi, H.L. Liu, Adsorption behavior of bisphenol A on sediments in Xiangjiang River, Central-south China, Chemosphere 65 (2006) 1490–1499.
[12] R. Baciocchi, M.R. Boni, R. Lavecchia, Modeling of chlorophenols competitive adsorption on soils by means of the ideal adsorbed solution theory, J. Hazard. Mater. 118 (2005) 239–246.
[13] S. Andini, R. Cioffi, F. Colangelo, F. Montagnaro, L. Santoro, Adsorption of chlorophenol, chloroaniline and methylene blue on fuel oil fly ash, J. Hazard. Mater. 157 (2008) 599–604.
[14] S.P. Kamble, P.A. Mangrulkar, A.K. Bansiwal, S.S. Rayalu, Adsorption of phenol and o-chlorophenol on surface altered fly ash based molecular sieves, Chem. Eng. J. 138 (2008) 73–83.
[15] D.S. Sun, X.D. Zhang, Y.D. Wu, X. Liu, Adsorption of anionic dyes from aqueous solution on fly ash, J. Hazard. Mater. 181 (2010) 335–342.
[16] Y.S. Liu, P. Liu, Z.X. Su, F.S. Li, F.S. Wen, Attapulgite-Fe_3O_4 magnetic nanoparticles via co-precipitation technique, Appl. Surf. Sci. 255 (2008) 2020–2025.
[17] Y. Liu, W. Jiang, S. Li, Z.P. Cheng, D. Song, X.J. Zhang, F.S. Li, Attachment of magnetic nanoparticles on carbon nanotubes using oleate as an interlinker molecule, Mater. Chem. Phys. 116 (2009) 438–441.
[18] J. Cao, X.W. Liu, R. Fu, Z.Y. Tan, Magnetic P zeolites: synthesis, characterization and the behavior in potassium extraction from seawater, Sep. Purif. Technol. 63 (2008) 92–100.
[19] H.Y. Zhu, R. Jiang, L. Xiao, G.M. Zeng, Preparation, characterization, adsorption kinetics and thermodynamics of novel magnetic chitosan enwrapping nanosized γ-Fe_2O_3 and multi-walled carbon nanotubes with enhanced adsorption properties for methyl orange, Bioresour. Technol. 101 (2010) 5063–5069.
[20] H.Y. Zhu, R. Jiang, L. Xiao, W. Li, A novel magnetically separable γ-Fe_2O_3/crosslinked chitosan adsorbent: preparation, characterization and adsorption application for removal of hazardous azo dye, J. Hazard. Mater. 179 (2010) 251–257.
[21] X. Wang, L.Y. Wang, X.W. He, Y.K. Zhang, L.X. Chen, A molecularly imprinted polymer-coated nanocomposite of magnetic nanoparticles for estrone recognition, Talanta 78 (2009) 327–332.
[22] R. Gtmez-villacieros, L. Heman, J. Morales, J.L. Tirado, Textural evolution of synthetic γ-FeOOH during thermal treatment by differential scanning calorimetry, J. Colloid Interface Sci. 101 (1984) 392–400.
[23] T.S. Zhang, H.M. Luo, H.X. Zeng, R.F. Zhang, Y.S. Shen, Synthesis and gas sensing characteristics of high thermostability γ-Fe_2O_3 power, Sens. Actuators (1996) B181–B184.
[24] M. Sathishkumar, A.R. Binupriya, D. Kavitha, R. Selvakumar, R. Jayabalan, J.G. Choi, S.E. Yun, Adsorption potential of maize cob carbon for 2,4-dichlorophenol removal from aqueous solutions: equilibrium, kinetics and thermodynamics modeling, Chem. Eng. J. 147 (2009) 265–271.
[25] J.M. Pan, X.H. Zou, X. Wang, W. Guan, Y.S. Yan, J. Han, Selective recognition of 2, 4-dichlorophenol from aqueous solution by uniformly sized molecularly imprinted microspheres with β-cyclodextrin/attapulgite composites as support, Chem. Eng. J. 162 (2010) 910–918.
[26] M. Mazzotti, Equilibrium theory based design of simulated moving bed processes for a generalized Langmuir isotherm, J. Chromatogr. A 1126 (2006) 311–322.
[27] Z. Alqodah, Adsorption of dyes using shale oil ash, Water Res. 34 (2000) 4295–4303.
[28] Y.S. Ho, G. McKay, The sorption of lead(II) ions on peat, Water Res. 33 (1999) 578–584.
[29] Y.S. Ho, G. McKay, Pseudo-second order model for sorption processes, Process Biochem. 34 (1999) 451–465.
[30] C.H. Weng, Y.F. Pan, Adsorption of a cationic dye (methylene blue) onto spent activated cay, J. Hazard. Mater. 144 (2007) 355–362.
[31] A.E. Ofomaja, Sorption dynamics and isotherm studies of methylene blue uptake on to palm kernel fibre, Chem. Eng. J. 126 (2007) 35–43.
[32] A.E. Ofomaja, Kinetic study and sorption mechanism of methylene blue and methyl violet onto mansonia (*Mansonia altissima*) wood sawdust, Chem. Eng. J. 143 (2008) 85–95.
[33] A.E. Ofomaja, Intraparticle diffusion process for lead(II) biosorption onto mansonia wood sawdust, Bioresour. Technol. 101 (2010) 5868–5876.
[34] A.E. Ofomaja, Y.S. Ho, Effect of pH on cadmium biosorption by coconut copra meal, J. Hazard. Mater. 139 (2007) 356–362.
[35] A. Kumar, S. Kumar, S. Kumar, D.V. Gupta, Adsorption of phenol and 4-nitrophenol on granular activated carbon in basal salt medium: equilibrium and kinetics, J. Hazard. Mater. 147 (2007) 155–166.
[36] W.M.I. Alvin, P.B. John, G. Mckay, A comparative study on the kinetics and mechanisms of removal of Reactive Black 5 by adsorption onto activated carbons and bone char, Chem. Eng. J. 157 (2010) 434–442.
[37] S.J. Allen, G. Mckay, J.F. Porter, Adsorption isotherm models for basic dye adsorption by peat in single and binary component systems, J. Colloid Interface Sci. 280 (2004) 322–333.
[38] C.P. Dwivedi, J.N. Sahu, C.R. Mohanty, B.R. Mohan, B.C. Meikap, Column performance of granular activated carbon packed bed for Pb(II) removal, J. Hazard. Mater. 156 (2008) 596–603.
[39] A.E. Ofomaja, E.I. Unuabonah, N.A. Oladoja, Competitive modeling for the biosorptive removal of copper and lead ions from aqueous solution by Mansonia wood sawdust, Bioresour. Technol. 101 (2010) 3844–3876.
[40] J.M. Pan, X.H. Zou, X. Wang, W. Guan, C.X. Li, Y.S. Yan, X.Y. Wu, Adsorptive removal of 2,4-didichlorophenol and 2,6-didichlorophenol from aqueous solution by β-cyclodextrin/attapulgite composites: equilibrium, kinetics and thermodynamics, Chem. Eng. J. 166 (2011) 40–48.
[41] T. Sismanoglu, Y. Kismir, S. Karakus, Single and binary adsorption of reactive dyes from aqueous solutions onto Clinoptilolite, J. Hazard. Mater. 184 (2010) 164–169.
[42] S.E. Diltemiz, R. Say, S. Büÿuktiryaki, D. Hür, A. Denizli, A. Ersöz, Quantum dot nanocrystals having guanosine imprinted nanoshell for DNA recognition, Talanta 75 (2008) 890–896.
[43] X.H. Gu, R. Xu, G.L. Yuan, H. Lu, B.R. Gu, H.P. Xie, Preparation of chlorogenic acid surface-imprinted magnetic nanoparticles and their usage in separation of traditional Chinese medicine, Anal. Chim. Acta 675 (2010) 64–70.